5-25-2023

Design and Implementation of Montmorillonite Clay-Based Catalyst for Carbon Nanotube Synthesizing

Mohamed Morsy
mohamed.morsy@bue.edu.eg

Solid State Phenomena
ISSN: 1662-9779, Vol. 342, pp 37-50

Submitted: 2023-02-06
Revised: 2023-02-12
Accepted: 2023-02-12
Online: 2023-05-25

Design and Implementation of Montmorillonite Clay-Based Catalyst for Carbon Nanotube Synthesizing

Mohamed Morsy[1,2,a*], H. Shoukry[1,b], Mahmoud Gharieb[3,c], Abdeen M. El-Nagar[3,d], W.M. Taha[4,e] and M.M. Mokhtar[1,f]

[1]Building Physics and Environment Institute, Housing & Building National Research Center (HBRC), Dokki, Giza, 12311, Egypt.

[2]Nanotechnology Research Centre (NTRC), The British University in Egypt (BUE), Suez Desert Road, El-Sherouk City, Cairo, 11837, Egypt

[3]Raw Building Materials Technology and Processing Research Institute, Housing & Building National Research Center (HBRC), Giza, Egypt

[4]Physics Department, Faculty of Women for Arts, Science and Education, Ain Shams University, Cairo 11757, Egypt

[a]83morsy@gmail.com, [b]hamadashoukry@yahoo.com, [c]medo_20109129@yahoo.com, [d]abdeenelnagar@yahoo.com, [e]walaataha505@gmail.com, [f]mmahmoud7@gmail.com

Keywords: clay; carbon nanotube; TEM; Raman; FTIR; XRD

Abstract. In this study, a catalyst based on Montmorillonite clay was implemented for carbon nanotubes (CNTs) synthesizing. The kaolinite clay was used as a supporting material for iron-cobalt bimetallic catalytic nanoparticles. The CNTs have been synthesized by using atmospheric chemical vapor deposition (APCVD). To assess the quality of preparation both the catalyst and CNTs have been characterized by different techniques. The chemical bonding and interactions were verified by FT-IR. The general overview of microstructure was examined using SEM, while, the detailed structure and morphology were examined by HR-TEM, in addition to thermal analysis (DTA); surface area (BET); X-ray fluorescence (XRF), Raman spectroscopy, and XRD analysis. The results revealed that; Fe_2O_3 and Co_3O_4 NPs were uniformly assembled on the clay nanoplatelets. The specific BET surface area of the clay and catalyst was determined to be 46.12 and 57.06 m^2/g respectively. Also, from XRD, the peaks at 26° and 42.7° confirm the presence of CNTs. The FTIR absorption bands, D, G, and G\ bands from the Raman spectrum confirm the hexagonal structure of the CNTs. The obtained results prove the high quality of CNTs preparation.

1- Introduction

The utilization of carbon nanotubes (CNTs) became essential in diverse applications due to their outstanding properties [1–4]. These applications cover all our life aspects that cannot be stated here in detail. Some of these applications include biomedical applications [5], sensors and transducers [6] [7], battery [8], energy harvesting [9], electromagnetic wave shielding [10], reinforcement of cementitious and polymer materials [11], human health monitoring [12], hydrogen storage [13], drug carriers [14], and water treatment [15]. Due to the growing areas of applications that use CNTs, many synthesizing methods have been proposed. These proposed methods comprises three main routes for CNTs synthesizing which are arc discharge, laser ablation and chemical vapor deposition [16]. Despite the advantages and disadvantages of the above-mentioned routs, chemical vapor deposition (CVD) is the most promising and scalable method [17]. The advantages of CVD are directly related to its scalability, ease of control, and low production cost. Additionally, it can be adapted easily for producing different forms of CNTs. Moreover, huge quantities of CNTs can be synthesized via CVD [18–20].

CNTs require catalyst materials capable of breaking up hydrocarbon to its individual constituents, then depositing it as hollow nano-sized fiber. The catalyst material has the leading role in decomposing hydrocarbon, and growing CNTs in a cylindrical form, controlling diameter and length, and determining its chirality as well. The catalyst composed of two main components which

are metallic nanoparticles deposited over supporting material [21] [16]. Many studies have been examined Ni, Co, and Fe with supports such as SiO_2 and Al_2O_3 as optimum catalyst for producing high yield CNTs with reasonable price [22]. Iron one of the most targeted catalysts due to their abundant, low price, nontoxicity, high carbon solubility and d orbital vacancies [23,24]. Different sources of iron comprise $FeCl_2$, $Fe(NO_3)_2$, $FeSO_4$ and $FePO_4$ are commonly utilized as catalysts for CNTs synthesizing. Iron nitrate catalysts precursors prove a high yield production of CNTs. The combination between Fe and Co were found more effective for producing high yield of CNTs. Al-Fatesh et al reported the performance of the Fe/Al_2O_3, $Co\text{-}Fe/Al_2O_3$, $Ni\text{-}Fe/Al_2O_3$ as a catalyst for CNTs. Their results demonstrate that among all investigated catalyst, $Co\text{-}Fe/Al_2O_3$ is the best among all of the tested catalyst [25]. The effect of amount of iron loaded over MgO on the formation of single wall carbon nanotubes (SWCNTs) and double wall carbon nanotube (DWCNTs) has been investigated. The obtained results confirmed the correlation between the amount of loaded Fe catalyst and type of produced CNTs. For low concentration of Fe, SWCNTs is favored, with increasing the Fe up to 3%, DWCNTs formed [26]. The bimetallic catalyst composed of Fe and Co demonstrates a high production yield of CNTs compared to Ni containing catalyst as confirmed by Awadallah et al. [27]. Clay minerals have been explored as a support material for CNTs synthesizing. The advantages of using clays is belonging to its ion exchange properties, unique swelling, and intercalation properties, so that the clays can easily and uniformly loaded with metallic nanoparticles [28,29]. In this research, nano metakaolin (NMK) decorated with bi metallic Fe and Co has been prepared using impregnation method for CNTs production using CVD. The effect of hydrocarbon flow rate on the quality of the synthesized CNTs has been examined. The hydrocarbon flow rate was set at different three values of 10, 30 and 50 ml/min. The structure, morphology, and quality of the deposited carboniuos materials have been investigated. Many techniques such as XRD, FTIR, Raman, SEM, and HRTEM confirmed the formation of CNTs.

2- Experimental

2.1. Materials

Iron nitrate nonahydrate was purchased from sigma Aldrich. Cobalt nitrate and Ammonium chloride were obtained from Fisher, Montmorillonite clay was purchased from our local market.

2.2. Catalysis preparation

The catalysis is composed of catalytic nanoparticles and support material. the kaolinite clays have been used as a support material, as they offer high metal dispersion and prevented metal nanoparticles from agglomeration.

10 gm of exfoliated nano metakaolin were suspended in 50 ml of de-ionized water via ultrasonication for 1h and then, stirred for an additional 1h. In a parallel beaker, 6 g of cobalt nitrate and 7 g of iron nitrate were dissolved in 50 ml of de-ionized water for 30 min under continuous stirring. The two solutions are mixed and stirred for 3 h, after that the water of the resulted solution was evaporated overnight at 120 °C. Finally, the obtained powder was calcined at 350 °C for 2 h and crushed into fine powder. The obtained dark brown powder is stored in a dry environment. The schematic representation of catalysis preparation is illustrated in fig. 1a.

2.3. CNTs synthesizing:

CNTs have been synthesized by atmospheric chemical vapor deposition (APCVD) method using iron-cobalt bimetallic as a catalyst supported over exfoliated NMK as shown schematically in fig. 1b.

The synthesizing method has been executed as follows:

2 gm of catalytic nanoparticles have been loaded in a quartz boat and inserted at the middle of the CVD furnace. The temperature of the CVD furnace was adjusted to 750 °C, and Nitrogen gas allowed to flow at 50 ml/min for 30 min to remove oxygen species and impurities. When reaching the target temperature (750°), the acetylene gas was allowed to flow at 10ml/min for 30 min. As the

synthesizing time elapsed, the CVD cooled down to room temperature under the protection of nitrogen flow until reaching room temperature. The previous two steps were repeated two times at different flow rates of acetylene gas (30 and 50ml/min). Finally, the deposited black powder was collected for further characterization

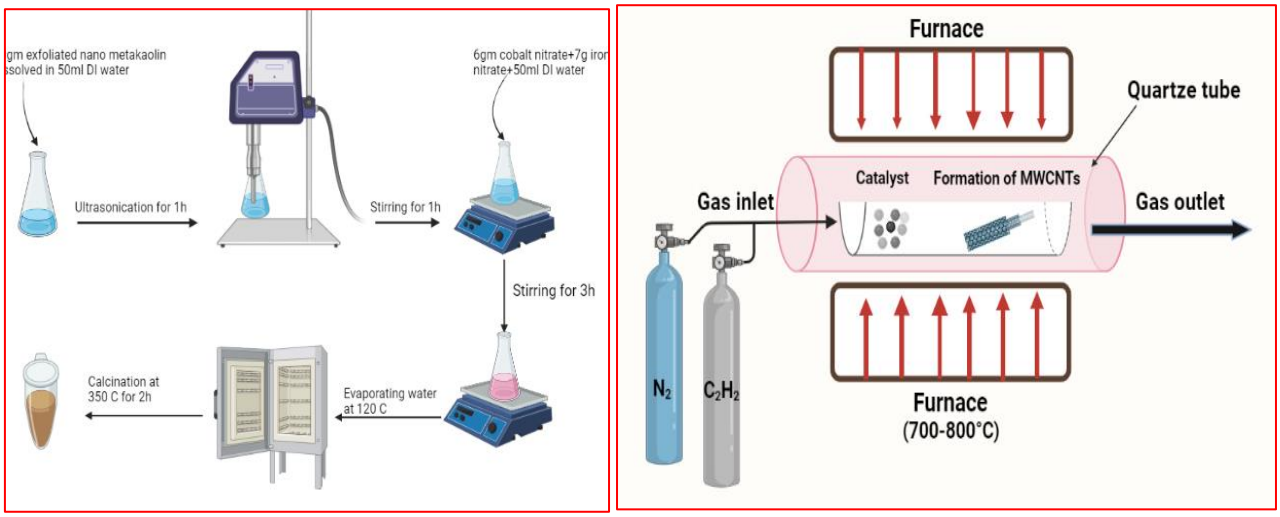

Figure 1: a) Schematic representation for the catalysis preparation and b) Schematic diagram of APCVD reactor

2.4. Characterization techniques:

The utilized tools for characterizing both catalyst and deposited carbonous materials are as follows:

- The X-ray diffraction (XRD) patterns of support and catalyst were collected by Malvern Panalytical Empyrean 3 diffractometer using CuKα radiation (λ = 1.54 A°) to confirm the phase composition and crystal structure.
- The chemical bonding and interactions were verified by FT-IR measurements. The FTIR spectra were recorded in a spectral range of 4000–400 cm^{-1} with a spectral resolution of 4 cm^{-1} using FT-IR spectrometer (Vertex 70, Bruker).
- The general overview of microstructure examined using SEM, thermos scientific, operated at 20 kV.
- Chemical analysis of the raw materials was carried out using Axios [(PW4400) WD-XRF] Sequential Spectrometer.
- The Brunauer-Emmett-Teller (BET) surface area was determined using Quanta chrome NOVA 2200E BET by N2 adsorption.
- The detailed structure and morphology were examined by High Resolution Transmission Electron Microscope (HR-TEM), JEM-2100 operated at 200 kV.
- The Raman spectrum was collected by Witec Alpha 300 RA, (514 nm excitation) instrument.

3- Results and Discussion

3.1. Catalyst

The phase composition and structure of NMK as a supportive material and catalyst were identified by x-ray diffraction (XRD) measurement as presented in fig. 2.

The main constituents of NMK are silica, followed by alumina, which accounts for more than 60% of its total composition. The diffraction peaks of NMK at 2θ equal 12.2º, and 24.7º, are indexed to (001) and (002) diffraction planes of aluminum silicate hydrate (ASH) which coincided with card No. 00-058-2006. The diffraction peaks at 21.2º, can be indexed to (001) crystallographic plane of alumina **[6].** The peak at 26.6º is attributed to the presence of the silicon dioxide (quartz) which matched with card No. 01-089-1961. The diffraction pattern of the catalyst has approximately the same diffraction peaks beside additional peaks related to the presence of catalytic

metal oxide nanoparticles. It can be observed that the intensity of the catalyst diffraction pattern is enhanced due to the loading of nanoparticles.

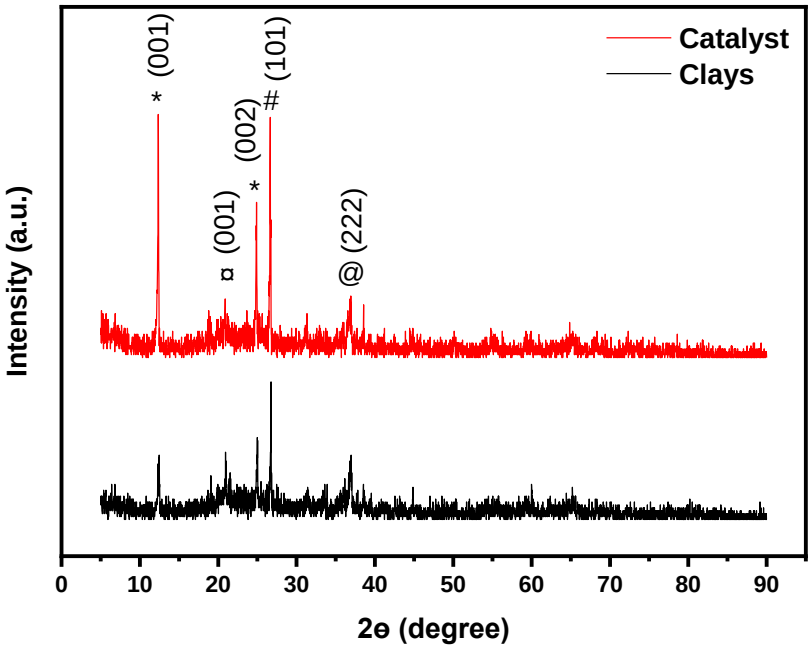

Figure 2: The XRD pattern of NMK and the catalyst

FTIR absorption bands of NMK and catalyst material is illustrated in fig. 3. NMK has absorption bands between 3500 and 3750 cm^{-1} corresponding to stretching vibration of OH groups. The presence of 3621 and 3685 cm^{-1} absorption band demonstrates the disordered structure of the kaolinite **[7]**. The band at 1005, 457, 428 cm^{-1} is associated with (Si-O) in agreement with Chakchouk et al. (2009) **[8].**

Bands at 914, and 791 cm^{-1} of NMK are attributed to (Al–OH) hydroxyl groups. Some peaks were found in the range of 667 cm^{-1} and 574 cm^{-1} in the FTIR spectrum due to the presence of cobalt oxide nanoparticles, which represented the synthesis of cobalt oxide nanoparticles **[9].** The Doublet of quartz appears at wave number of 781 and 785 cm^{-1}. The band at 681 is corresponding to the Si-O-Si of quartz as confirmed earlier by XRD measurement, while the band at 528 cm^{-1} arises from the deformation vibrations Al VI-O-Si **[10].** For the catalyst, the bands that characterize NMK is existed. Shifting towards the lower frequency might resulted from the chemical bonding action between cobalt, iron and oxygen atoms **[11]** of additionally the presence of cobalt and iron species also identified. The assignment of the absorption bands in IR spectra of NMK is summarized in table 1.

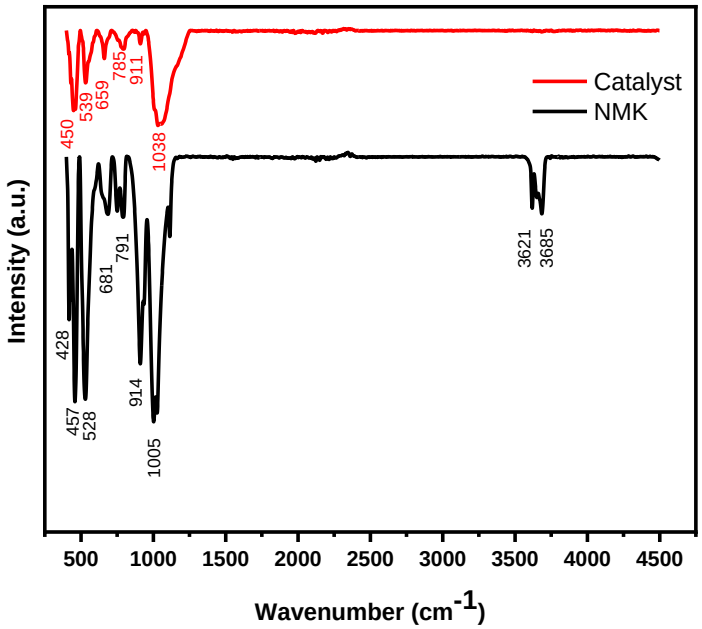

Figure 3: The FTIR pattern of NMK and the catalyst

Table 1: The assignment of the absorption bands in IR spectra of NMK

Assignment	Band location (cm^{-1})	Reference
OH stretching of outer surface hydroxyl groups (OutOH)	3685	**[12,13]**
Stretching mode of an inner hydroxyl group (InOH)	3621	**[12,13]**
Si - O in the plane	1005	**[14]**
Al–OH bending vibration	914	**[12]**
Presence of quartz: Si with basal oxygen	790	**[12]**
Si-O-Al^{VI} bending vibration	528	**[15]**
Si-O-Si bending deformation	457	**[15]**
Si-O bending vibrations	428	**[12,6]**

Figure 4 shows the SEM micrograph for the exfoliated NMK. The clay particles showed single crystalline hexagonal shaped nanosheets along with few nanoplatelets. The sheets seem to be separated that will facilitate the deposition of metallic nanoparticles over its surface. The associated EDX spectrum exhibited Si, Al and O as the main constituents which confirm the kaolinite type **[16, 17].**

Figure 5 shows the SEM micrograph for the $CoFe_2O_4$-modified NMK sheets. As it is clear, $CoFe_2O_4$ nanoparticles are uniformly spread on the NMK sheets. The morphology of $CoFe_2O_4$-modified clay nano sheets retains to a great extent the hexagonal nanosheet structure. The clay nano sheets with uniformly distributed $CoFe_2O_4$ nanoparticles could offer good quality catalyst. The EDS pattern confirmed the presence of Co and Fe elements on the clay nanosheet surface.

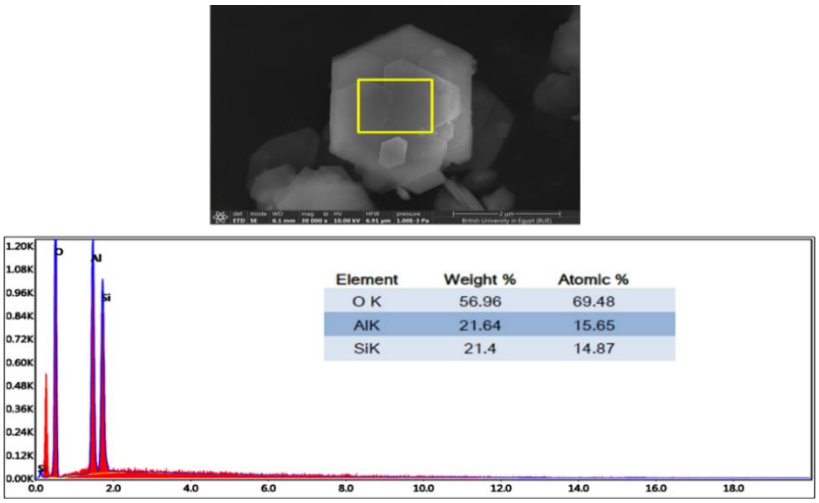

Figure 4: SEM and EDS analyses of NMK clay

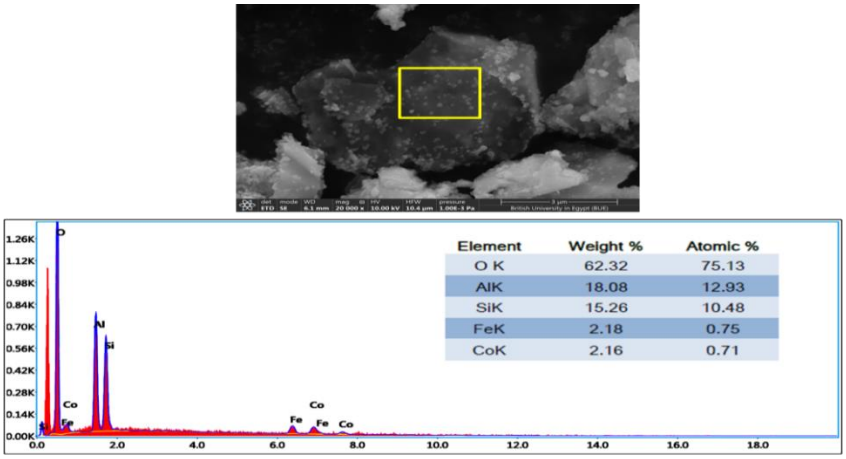

Figure 5: SEM and EDS analyses of $CoFe_2O_4$-modified NMK clay

Table 2 shows the chemical analysis (XRF) of clay and $CoFe_2O_4$-modified clay nano sheets (catalytic). As it is clear the clay without additives consists of silicon dioxide (SiO_2) and aluminum oxide (Al_2O_3). It could be seen from Table 2 that Fe_2O_3 and (Co_3O_4) NPs were successfully assembled on the clay platelets.

Table 2: Chemical composition of NMK and catalysis

Oxide Content	Catalytic	Clay
SiO_2	36.84	52.60
Al_2O_3	27.90	37.80
Fe_2O_3	11.00	0.47
CaO	0.44	0.36
Mgo	0.08	0.05
SO_3^{--}	0.48	0.34
L.O.I.	11.30	5.62
Na_2O	0.37	0.08
K_2O	0.09	0.08
TiO_2	0.99	1.45
Cl^-	0.10	0.11
Co_3O_4	9.68	-
P_2O_5	0.38	0.49
SrO	0.26	0.38
Total	99.99	99.97

The specific surface area of NMK and the catalyst samples were determined from the N_2 adsorption/desorption isotherms of the thermally and chemically exfoliated clay in addition to the catalyst sample are presented in fig. 6.

Generally, the hysteresis loop of the two samples presented in this figure is of type H3 according to the IUPAC classification [18], which is typical of particles with plate-like structures containing mesopores. The volume of the adsorbed nitrogen obtained from the isotherms is mostly dependent on the specific surface area. The catalyst sample adsorbed more nitrogen than the clay sample which interprets its higher surface area. The specific BET surface area of the clay and catalyst were determined to be 46.12 and 57.06 m^2/g respectively.

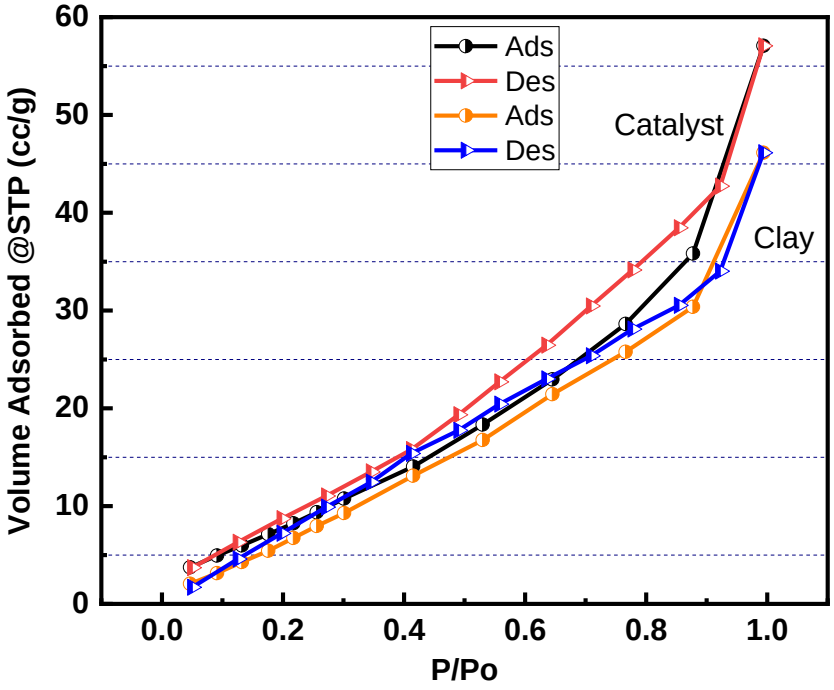

Figure 6: The N_2 adsorption/desorption isotherms for clay and catalyst

Fig.7 shows the HR-TEM representative images along with the selected area electron diffraction (SAED) patterns of pure and $CoFe_2O_4$-modified clay nanosheets respectively. As it is clear the pure clay possesses platelets like hexagonal structures with sharp-edged crystals. The clay nanosheets exhibited large length to thickness (aspect ratio); although their dimensions in length and width can be measured in hundreds of nanometers, the platelet thickness is <20 nm. It could be seen from fig.7(b) that $CoFe_2O_4$ NPs were successfully assembled on the clay platelets by preserving their initial particle size and morphology. A group of smaller $CoFe_2O_4$ NPs < 100 nm are distributed over the clay platelet surface.

The SAED pattern in Fig. 7 (a) showed clear diffraction spots which point to the high quality and hexagonal structured single-crystalline clay nanosheet. However, the Co-Fe-modified clay showed a dotted pattern of single-crystalline clay and a polycrystalline ring of Co_3O_4 and Fe_2O_3 nanoparticles.

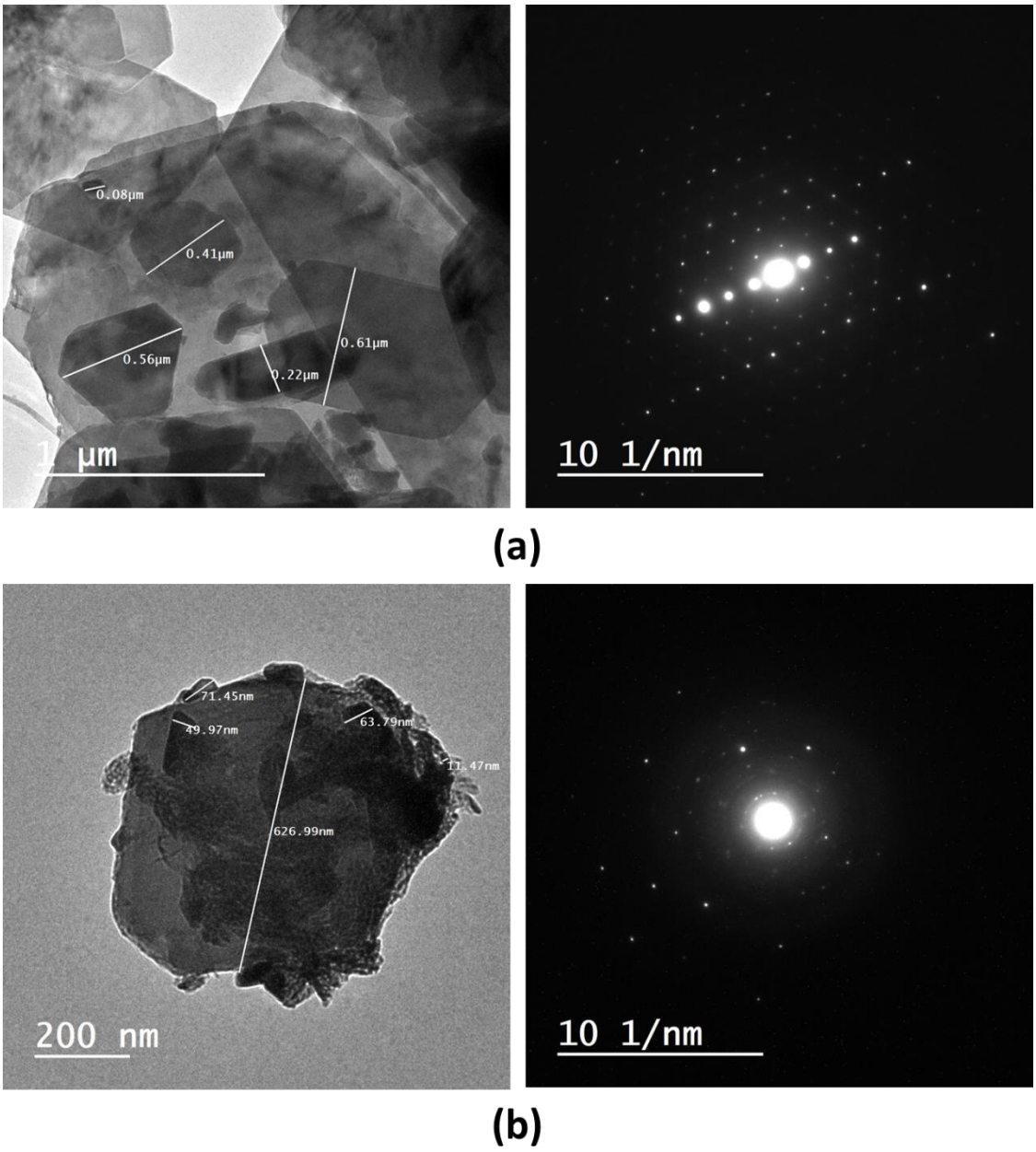

Figure 7: HR-TEM image and SAED pattern of (a) Pure clay and (b) $CoFe_2O_4$ NPs hosted in clay

3.2. MWCNTs synthesizing:

The phase composition of the synthesized materials was characterized by XRD. The XRD patterns of the T1, T2, and CNTs are depicted in Fig.8. the diffraction pattern of the T1 sample exhibited two peaks at 18.7 ° and 25.9°. The broad peak at 25.9° confirms the amorphous structure of the sample [30]. For the CNTs sample, two peaks can be recognized. The peaks at 26° and 42.7° are attributed to the diffraction planes of (002) and (004) of CNTs.

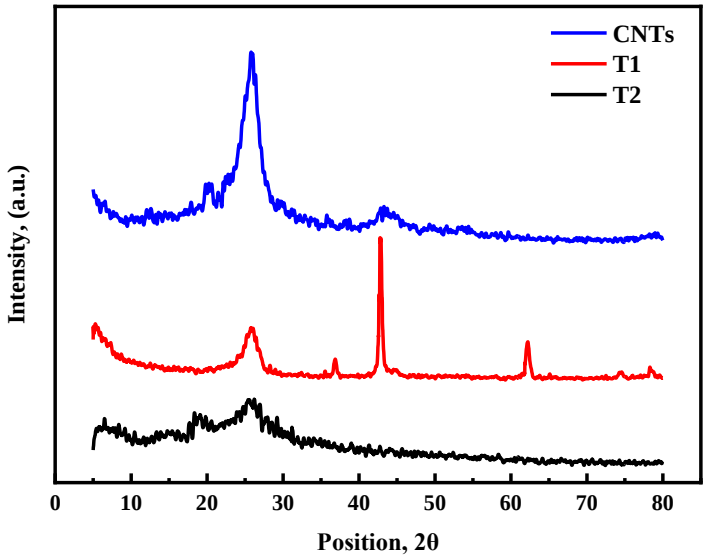

Figure 8: XRD pattern of the prepared samples; CNTs, T1 and T2

The FTIR, as a fast and powerful technique, has been utilized to confirm the formation of CNTs. The FTIR measurement was conducted on pristine sample before performing purification and functionalization. This was done to determine the forthcoming treatment procedures on a selected sample. The characteristic FTIR absorption bands of MWCNT prepared by cobalt-iron bi catalyst supported over nano clays in the spectral range from 400 up to 4500cm^{-1} is illustrated in Fig.9. MWCNTs have absorption bands between 3220cm^{-1} corresponding to stretching vibration of -OH groups which can be ascribed to the oscillation of carboxyl groups. The band at 1575 cm^{-1} is associated with the stretching of the carbon nanotube backbone, while the peak at 1299cm^{-1} is due to the C–C bond stretch. The band at 1151 cm^{-1} is associated with –C–O. Some peaks were found in the range of 1500 cm^{-1} and 1580 cm^{-1} corresponding to stretching of C–C indicates the presence of a carbon double bond (C=C); this finding confirms the hexagonal structure of the CNTs [31]. Some additional peaks were found in the range of 820 cm^{-1} to 450 cm^{-1} in the FTIR spectrum due to the presence of cobalt, oxide, and iron oxide nanoparticles. For T1 and T2 samples the presence of the formed bonds doesn't support the formation of the CNTs.

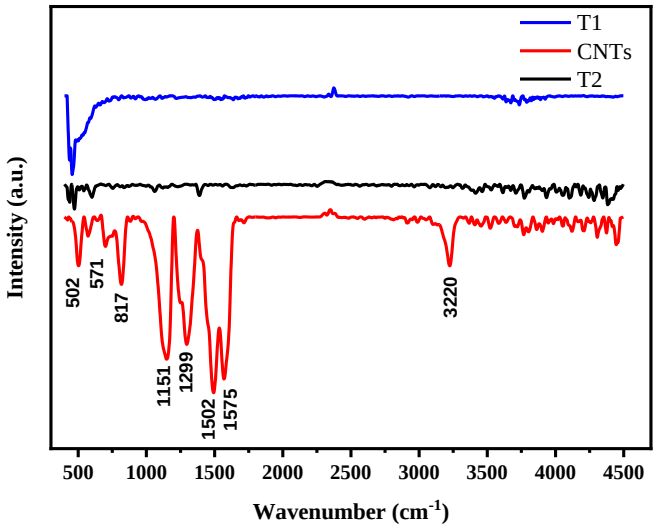

Figure 9: FTIR spectra of CNTs and trials T1 and T2

Raman spectroscopy is a powerful tool that used to study the ordered/disordered crystal structure of nanocarbon materials [32]. Fig.10 presents the Raman spectra of the prepared different carbon materials performed in the range of 50 – 4000 cm^{-1}. It obvious that, the obtained spectra show the well-known and stablished D (occurred due to the degree of disorder of a structure), G (occurred as a result of the degree of graphitization of the tubes) and 2D (which is related to stresses) bands characterizing the MWCNTs located at 1345cm^{-1}, 1580cm^{-1} and 2687 cm^{-1} respectively. In addition, the RBM (Radial Breathing Mode) bands that are usually located in the range of 150 - 200cm^{-1} are absence from the spectrum which is an additional proof for the presence of MWCNTs [33] [34]**.** For all of these, one can be certain from the preparation quality of MMWCNTs. Furthermore, the intensity ratio (I_D/I_G) provides a good indication to the degree of carbon material crystallinity this ratio was calculated to be 0.95.

Finally, the figure also contains two additional spectra for T1 and T2 samples which are related to carbon materials other than CNTs, these samples were the first and second trials of preparing CNTs.

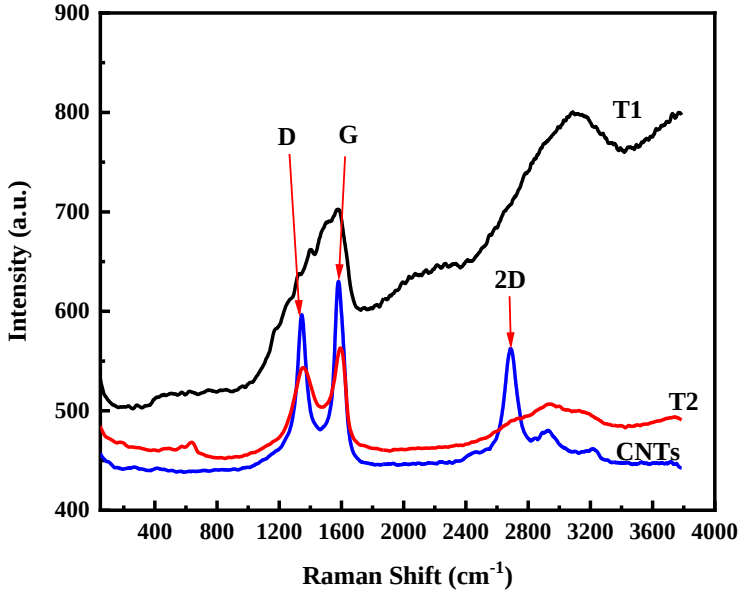

Figure 10: Raman spectrum of T1, T2 and CNTs samples.

Two attempts were made to produce CNTs with $CoFe_2O_4$-modified clay nano sheets as catalyst. As shown from SEM and TEM in Fig. 11 (a & b) the CNTs synthesized in the first attempt were agglomerated and tightly compacted, i.e., they exhibited compact fiber clusters. This testifies that no adequate growth of CNT formation was occurred. In addition, spherical solid particles are obvious in SEM and confirmed at higher magnifications by TEM. The poisoning of the catalyst as a result of high flow rate of acetylene may explain the improper growth of the prepared CNTs.

As seen in Fig. 12a, clear/ adequate growth of CNTs has been obtained in the 2nd attempt. Although, the SEM image demonstrated randomly oriented CNTs and some of them are entangled, the synthesized CNTs possessed uniform morphology. The HRTEM micrograph in Fig. 12b, showed a string-like individual CNTs, which are maulti-walled with inner diameter of about 11~19 nm.

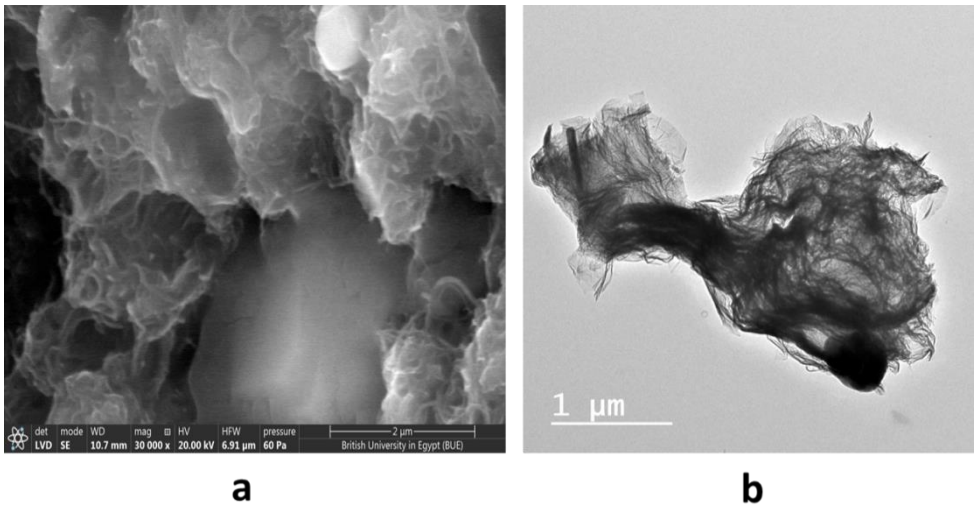

Figure 11: Morphology of CNTs prepared in 1st attempt as examined by (a) SEM and (b) TEM

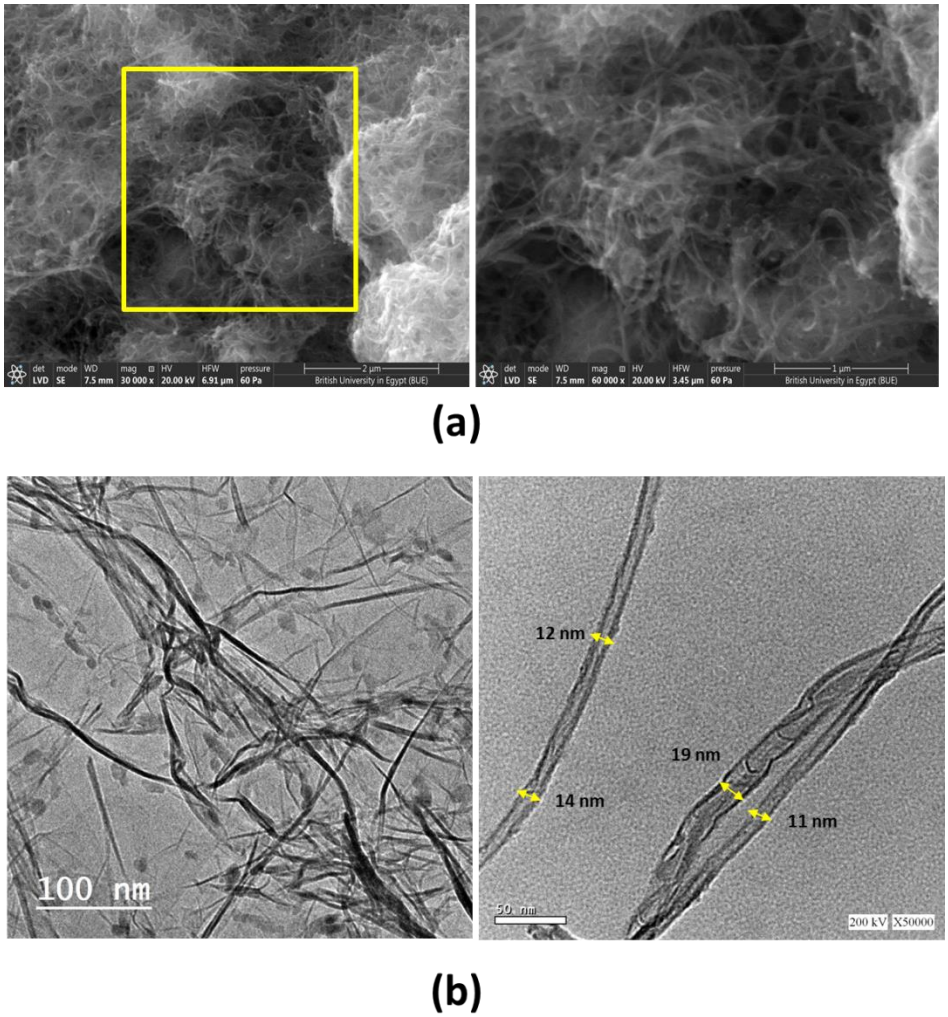

Figure 12: Morphology of CNTs prepared in 2nd attempt as examined by (a) SEM and (b) TEM

4. Conclusions

In this study, $CoFe_2O_4$-modified clay nano sheets as bimetallic catalytic has been effortlessly prepared for unique carbon nanotube synthesizing; based on the experimental results, the following conclusions can be drawn:

- The Fe_2O_3 and Co_3O_4 nano particles assembled on the clay platelets exhibited an enhanced specific surface area of the bimetallic catalyst. BET surface area of about 57.06 m^2/g has been obtained.
- The uniform distribution of $CoFe_2O_4$ nanoparticles on the clay hexagonal nano sheets has been confirmed by SEM analysis which points to the high quality of the newly developed catalyst.
- The CNTs prepared with $CoFe_2O_4$-modified clay nano sheets as catalyst are maulti-walled with inner diameter of about 11~19 nm.
- The obtained Raman spectra showed a significant degree of graphitization of the tubes and provided a proof for the presence of MWCNTs.

Acknowledgement

- The authors would like to thank the science, technology, and innovation funding authority (STDF) for financial funding this work through the project ID:37105.

References

[1] M. Morsy, M. Helal, M. El-Okr, M. Ibrahim, Preparation and characterization of multiwall carbon nanotubes decorated with zinc oxide, Der Pharma Chemica. 7 (2015).

[2] C. Nano, B. Materials, Egyptian Journal of Chemistry, 65 (2022) 691–714. doi:10.21608/ejchem.2021.99842.4641.

[3] M. Morsy, M. Helal, M. El-Okr, M. Ibrahim, Preparation, purification and characterization of high purity multi-wall carbon nanotube, Spectrochimica Acta - Part A: Molecular and Biomolecular Spectroscopy. 132 (2014). doi:10.1016/j.saa.2014.04.122.

[4] A. Thakur, R. Bharti, R. Sharma, Carbon nanotubes: Types, synthesis, cytotoxicity and applications in biomedical, Materials Today: Proceedings. 50 (2022) 2256–2268. doi:https://doi.org/10.1016/j.matpr.2021.10.002.

[5] M.R.M. Radzi, Y.S. Yee, M.P. Yan, N.A. Johari, W.F.A.W.M. Zawawi, F.A. Lubis, N.A.M. Hendri, L.S. Raj, K. Jemon, Polyethylene glycol modified-carbon nanotubes as materials for biomedical applications: In vitro and in vivo sub-acute toxicity evaluation, Materials Letters. 326 (2022) 132979. doi:https://doi.org/10.1016/j.matlet.2022.132979.

[6] M. Morsy, I.S. Yahia, H.Y. Zahran, F. Meng, M. Ibrahim, Portable and Battery Operated Ammonia Gas Sensor Based on CNTs/rGO/ZnO Nanocomposite, Journal of Electronic Materials. 48 (2019). doi:10.1007/s11664-019-07550-7.

[7] M. Morsy, A.I. Abdel-Salam, M. Mostafa, A. Elzwawy, Promoting the humidity sensing capabilities of titania nanorods/rGO nanocomposite via de-bundling and maximizing porosity and surface area through lyophilization, Micro and Nano Engineering. 17 (2022) 100163. doi:https: //doi.org/10.1016/j.mne.2022.100163.

[8] X. Li, C. Xue, Y. Liu, J. Zhao, J. Zhang, J. Zhang, Amorphous structure and sulfur doping synergistically inducing defect-rich short carbon nanotubes as a superior anode material in lithium-ion batteries, Electrochimica Acta. 440 (2023) 141697. doi:https://doi.org/10.1016/j.electacta.2022.141697.

[9] H. Kim, J.W. Park, J.S. Hyeon, H.J. Sim, Y. Jang, Y. Shim, C. Huynh, R.H. Baughman, S.J. Kim, Electrical energy harvesting from ferritin biscrolled carbon nanotube yarn, Biosensors and Bioelectronics. 164 (2020) 112318. doi:https://doi.org/10.1016/j.bios.2020.112318.

[10] C. Wu, Y. Qu, Y. Wen, S. Gong, Z. Zhu, Cu and Fe bimetallic heterostructure nanoparticles supported by carbon nanotube for multilayer structure electromagnetic interference shielding composite, Composite Structures. 305 (2023) 116543. doi: https: //doi.org/ 10.1016/j.compstruct.2022.116543.

[11] M. Morsy, H. Shoukry, M.M. Mokhtar, N.A. Taha, M.S. Morsy, Systematic investigation into mechanical strength, pore structure and microstructure of high performance concrete incorporating nano-hybrids, IOP Conference Series: Materials Science and Engineering. 956 (2020). doi:10.1088/1757-899X/956/1/012001.

[12] W. Li, L.-Q. Tao, M.-C. Kang, C.-H. Li, C.-Y. Luo, G. He, T.-Y. Sang, P. Wang, Tunable mechanical, self-healing hydrogels driven by sodium alginate and modified carbon nanotubes for health monitoring, Carbohydrate Polymers. 295 (2022) 119854. doi:https: //doi.org/10.1016/j.carbpol.2022.119854.

[13] J.F.N. Dethan, V. Swamy, Mechanical and thermal properties of carbon nanotubes and boron nitride nanotubes for fuel cells and hydrogen storage applications: A comparative review of molecular dynamics studies, International Journal of Hydrogen Energy. 47 (2022) 24916–24944. doi:https://doi.org/10.1016/j.ijhydene.2022.05.240.

[14] G. Gul, R. Faller, N. Ileri-Ercan, Polystyrene-modified carbon nanotubes: Promising carriers in targeted drug delivery, Biophysical Journal. 121 (2022) 4271–4279. doi:https: //doi.org/10.1016/j.bpj.2022.10.014.

[15] M. Morsy, A.I. Abdel, D.A. Rayan, I. Gomaa, A. Elzwawy, Oil / water separation and functionality of smart carbon nanotube – titania nanotube composite, Journal of Nanoparticle Research. (2022) 1–15. doi:10.1007/s11051-022-05597-y.

[16] F. Han, L. Qian, Q. Wu, D. Li, S. Hao, L. Feng, L. Xin, T. Yang, J. Zhang, M. He, Narrow-chirality distributed single-walled carbon nanotube synthesized from oxide promoted Fe–SiC catalyst, Carbon. 191 (2022) 146–152. doi:https://doi.org/10.1016/j.carbon.2022.01.052.

[17] X. Yuan, C. Liang, C. Ruan, Y. Chang, L. Xu, H. Huang, M. Chen, Z. Yong, Low-cost synthesis of multi-walled carbon nanotubes using red soil as catalyst, Diamond and Related Materials. 112 (2021) 108241. doi:https://doi.org/10.1016/j.diamond.2021.108241.

[18] S. Ahmad, E.-X. Ding, Q. Zhang, H. Jiang, J. Sainio, M. Tavakkoli, A. Hussain, Y. Liao, E.I. Kauppinen, Roles of sulfur in floating-catalyst CVD growth of single-walled carbon nanotubes for transparent conductive film applications, Chemical Engineering Journal. 378 (2019) 122010. doi:https://doi.org/10.1016/j.cej.2019.122010.

[19] I. V Novikov, E.M. Khabushev, D. V Krasnikov, A. V Bubis, A.E. Goldt, S.D. Shandakov, A.G. Nasibulin, Residence time effect on single-walled carbon nanotube synthesis in an aerosol CVD reactor, Chemical Engineering Journal. 420 (2021) 129869. doi:https://doi.org/10.1016/j.cej.2021.129869.

[20] J. Lin, H. Jin, X. Ge, Y. Yang, G. Huang, J. Wang, F. Li, H. Li, S. Wang, Investigation of the parameters of carbon nanotube growth on zirconium diboride supported Ni catalyst via CVD, Diamond and Related Materials. 115 (2021) 108347. doi: https: //doi.org/10.1016/j.diamond.2021.108347.

[21] M. Morsy, A. Elzwawy, M. Oraby, Carbon Nano Based Materials and Their Composites for Gas Sensing Applications: Review, Egyptian Journal of Chemistry. 65 (2022) 591–614. doi: 10.21608/ejchem.2021.99842.4641.

[22] H. Wang, G. Gu, Q. Chen, X. Feng, Y. Chen, Cobalt sulfide catalysts for single-walled carbon nanotube synthesis, Diamond and Related Materials. 114 (2021) 108288. doi:https: //doi.org/10.1016/j.diamond.2021.108288.

[23] A.M. El Nahrawy, B.A. Hemdan, A.M. Mansour, A. Elzwawy, A.B. Abou Hammad, Integrated use of nickel cobalt aluminoferrite/Ni2+ nano-crystallites supported with SiO2 for optomagnetic and biomedical applications, Materials Science and Engineering: B. 274 (2021) 115491. doi:https://doi.org/10.1016/j.mseb.2021.115491.

[24] X.-X. Lim, S.-C. Low, W.-D. Oh, A critical review of heterogeneous catalyst design for carbon nanotubes synthesis: Functionalities, performances, and prospects, Fuel Processing Technology. 241 (2023) 107624. doi:https://doi.org/10.1016/j.fuproc.2022.107624.

[25] S. He, K. Seshan, ScienceDirect Production of hydrogen by catalytic methane decomposition over alumina supported mono- , bi- and tri-metallic catalysts, International Journal of Hydrogen Energy. 41 (2016) 22932–22940. doi:10.1016/j.ijhydene.2016.09.027.

[26] Z. Qiang, Z. Mengqiang, H. Jiaqi, Q. Weizhong, W.E.I. Fei, Selective Synthesis of Single / Double/Multi-walled Carbon Nanotubes on MgO-Supported Fe Catalyst, Chinese Journal of Catalysis. 29 (2008) 1138–1144. doi:10.1016/S1872-2067(09)60015-2.

[27] A.E. Awadallah, Applied Surface Science Catalytic thermal decomposition of methane to CO x -free hydrogen and carbon nanotubes over MgO supported bimetallic group VIII catalysts, Applied Surface Science. 296 (2014) 100–107. doi:10.1016/j.apsusc.2014.01.055.

[28] A. Destrée, G.J. Long, B. Vatovez, F. Grandjean, A. Fonseca, J.B. Nagy, A.-M. Fransolet, Synthesis and characterization of carbon nanotubes grown on montmorillonite clay catalysts, Journal of Materials Science. 42 (2007) 8671–8689. doi:10.1007/s10853-007-1808-2.

[29] D. Gournis, M.A. Karakassides, T. Bakas, N. Boukos, D. Petridis, Catalytic synthesis of carbon nanotubes on clay minerals, Carbon. 40 (2002) 2641–2646. doi:https: //doi.org/10.1016/S0008-6223(02)00165-3.

[30] S. Bose, S. Radhakrishnan, B.-S. Kim, H.W. Kang, Formulation of amorphous carbon embedded CuFeS2 hybrids for the electrochemical detection of Quercetin, Materials Today Chemistry. 26 (2022) 101228. doi:https://doi.org/10.1016/j.mtchem.2022.101228.

[31] R. Yudianti, H. Onggo, S. Sudirman, Y. Saito, T. Iwata, J.-I. Azuma, Analysis of Functional Group Sited on Multi-Wall Carbon Nanotube Surface, 5 (2010).

[32] H.-L. Guo, X.-F. Wang, Q.-Y. Qian, F.-B. Wang, X.-H. Xia, A Green Approach to the Synthesis of Graphene Nanosheets, ACS Nano. 3 (2009) 2653–2659. doi:10.1021/nn900227d.

[33] M. Science-poland, Characterization of carbon nanotubes by Raman spectroscopy, 26 (2008).

[34] A.D. Dobrzańska-Danikiewicz, D. Łukowiec, D. Cichocki, W. Wolany, Carbon nanotubes manufacturing using the CVD equipment against the background of other methods, Archives of Materials Science and Engineering. 64 (2013) 103–109.